Geomech. Geophys. Geo-energ. Geo-resour. (2024) 10:181
https://doi.org/10.1007/s40948-024-00897-0

RESEARCH

Splitting tensile strength of shale cores: intact versus fractured and sealed with ureolysis-induced calcium carbonate precipitation (UICP)

Kayla Bedey · Matthew R. Willett · Dustin Crandall · Jonny Rutqvist · Kirsten Matteson · Adrienne J. Phillips · Alfred B. Cunningham · Catherine M. Kirkland

Received: 2 April 2024 / Accepted: 18 October 2024

Abstract Ureolysis-induced calcium carbonate precipitation (UICP) is a biomineral solution where the urease enzyme converts urea and calcium into calcium carbonate. The resulting biomineral can bridge gaps in fractured shale, reduce undesired fluid flow, limit fracture propagation, better store carbon dioxide, and potentially enhance well efficiency. The mechanical properties of shale cores were investigated using a modified Brazilian indirect tensile strength test. An investigation of intact shale using Eagle Ford and Wolfcamp cores was conducted at varying temperatures. Results show no significant difference between shale types (average tensile strength = 6.19 MPa). Eagle Ford displayed higher strength at elevated temperature, but temperature did not influence Wolfcamp. Comparatively, cores with a single, lengthwise heterogeneous fracture were sealed with UICP and further tested for tensile strength. UICP was delivered via a flow-through method which injected 20–30 sequential patterns of ureolytic microorganisms and UICP-promoting fluids into the fracture until permeability reduced by three orders of magnitude or with an immersion method which placed cores treated with guar gum and UICP-promoting fluids into a batch

K. Bedey (✉) · K. Matteson · A. J. Phillips · A. B. Cunningham · C. M. Kirkland (✉)
Department of Civil Engineering, Montana State University, 205 Cobleigh Hall, Bozeman, MT 59717, USA
e-mail: kaylabedey@montana.edu

C. M. Kirkland
e-mail: catherine.kirkland@montana.edu

K. Matteson
e-mail: kirsten.matteson@montana.edu

A. J. Phillips
e-mail: adrienne.phillips@montana.edu

A. B. Cunningham
e-mail: al_c@montana.edu

K. Bedey · M. R. Willett · A. J. Phillips · A. B. Cunningham · C. M. Kirkland
Center for Biofilm Engineering, Montana State University, 366 Barnard Hall, Bozeman, MT 59717, USA
e-mail: matthewwillett@montana.edu

M. R. Willett
Department of Chemical Engineering, Montana State University, 214 Roberts Hall, Bozeman, MT 59717, USA

D. Crandall
National Energy Technology Laboratory, 3610 Collins Ferry Road, Mail Stop H06, Morgantown, WV 26507, USA
e-mail: Dustin.Crandall@NETL.DOE.GOV

J. Rutqvist
Lawrence Berkeley National Laboratory, 1 Cyclotron Road, MS 74R-316C, Berkeley, CA 94720, USA
e-mail: jrutqvist@lbl.gov

Published online: 13 November 2024

reactor, demonstrating that guar gum is a suitable inclusion and may reduce the number of flow-through injections required. Tensile results for both delivery methods were variable (0.15–8 MPa), and in some cores the biomineralized fracture split apart, possibly due to insufficient sealing and/or heterogeneity in the composite UICP-shale cores. Notably in other cores the biomineralized fracture remained intact, demonstrating more cohesion than the surrounding shale, indicating that UICP may produce a strong seal for subsurface application.

Article Highlights

- Sealing shale fractures with biomineralization can plug undesired fluid pathways and reduce possible greenhouse gas leakage.
- Biomineralization can strengthen fractured shale.
- The methods developed in this research, including the use of guar gum as an additive, are ready to be broadly applied to analyze multiple shale types in support of hydrocarbon recovery.

Keywords Shale · Biomineralization · Fracture sealing · Induced calcium carbonate precipitation · Splitting tensile strength · Brazilian tensile strength

1 Introduction

An abundance of natural gas (i.e., shale gas) is trapped within subsurface shale formations. Shale gas is an instrumental energy source and imperative to meeting global energy demands while the transition to economically feasible, climate-friendly alternative energy sources continues (Wang et al. 2014). Hydraulic fracturing (commonly known as fracking) coupled with horizontal drilling creates a fracture network within impermeable shale allowing access to otherwise inaccessible gas resources (Soeder 2018). While this technology continues to be instrumental in the evolving energy landscape, remediating the resulting fractures may be environmentally and economically advantageous.

Sealing fractures will reduce undesired leakage pathways that may lead to environmental impacts such as contaminating groundwater aquifers or methane leaking to the surface. Additionally, the low permeability of shale formations makes it an excellent geologic caprock layer above those targeted for carbon sequestration; however, if caprock layers are compromised, trapped carbon dioxide (CO_2) could migrate back into the atmosphere and thereby reduce the sequestration efficiency (Espinoza and Santamarina 2017; Rutqvist 2012). Furthermore, hydraulic fracturing recovers only a small percentage of available hydrocarbons, leaving behind excess resources in the not yet accessed rock (Kong et al. 2019). Re-fracturing the rock can aid in enhanced resource recovery by extending the life and efficiency of an existing well; however, this re-stimulation method contributes new fractures to the originally created network. Ureolysis-induced calcium carbonate precipitation (UICP) offers an innovative solution to seal fluid pathways in fractured shale. Unlike common fracture filling materials, like cement, UICP is advantageous because it utilizes microscopic cementing agents, low viscosity fluids, non-toxic constituents, and can penetrate microfractures.

1.1 UICP

During UICP, also known as biomineralization or bio-cementation, the hydrolysis of urea is catalyzed by the presence of the urease enzyme. When a calcium source is introduced, a calcium carbonate precipitate can form (Eq. 1) (Kirkland et al. 2021).

$$CO\left(NH_2\right)_2 + 2H_2O + Ca^{2+} \leftrightarrow 2NH_4^+ + CaCO_3(s) \quad (1)$$

A wide variety of bacteria, plants, and fungi produce the urease enzyme (Krajewska 2009; Mobley and Hausinger 1989; Stocks-Fischer et al. 1999). This study uses the ureolytic bacteria *Sporosarcina pasteurii* because it is non-pathogenic and contains high concentrations of urease (Phillips et al. 2013a). The engineering applications of UICP are wide ranging as reviewed by Phillips et al. (2013a). Subsurface application related to the work presented here include remediation related to hydraulic fracturing wells, enhanced oil and gas recovery, and improving caprock integrity for geologic carbon capture and storage (Phillips et al. 2013b). Significantly, UICP has been used in a variety of field applications for plugging undesired fluid pathways in wellbore cement (Kirkland et al. 2021, 2020; Phillips et al. 2016, 2018) and

sandstone fractures (Cuthbert et al. 2013). It has been shown to seal fractures in granite (Minto et al. 2016; Tobler et al. 2018) as well as fractured anhydrite with gouges (Sang et al. 2022). Biomineralization can repair cracks in concrete (Achal et al. 2013; Lu et al. 2023), as well as provide tensile strength recovery to fractured concrete building materials (Turner et al. 2023). UICP performed inside single-fractured sandstone specimen has been found to improve specimen mechanical properties and decrease fracture permeability (Deng et al. 2022; Yao et al. 2022). Moreover, UICP is well known to increase the compressive strength in unconsolidated, porous media like sand and soils (Cui et al. 2017; Ghasemi and Montoya 2022; Gomez et al. 2017; Halder et al. 2014; Lin et al. 2016; Montoya and DeJong 2015; Park et al. 2014; van Paassen et al. 2010; Whiffin et al. 2007; Xiao et al. 2019; Yasuhara et al. 2012). Further, UICP could be developed for fractured geothermal reservoirs for zonal isolation associated with reservoir stimulation and for sealing the widest so-called short-circuit fractures (Cladouhos et al. 2016; Petty et al. 2013). These studies show that UICP is successful in fracture sealing, permeability reduction, and geomechanical property modification.

1.2 UICP in fractured shale

Shale formations exist at elevated temperatures and increased pressures that pose challenges to the biochemical reaction governing UICP (Eq. 1). A few studies have explored the use of UICP in fractured shale and successfully produced biomineral precipitation inside shale fractures while mimicking subsurface conditions. Cunningham et al. (2015) biomineralized three Opalinus shale cores, two at ambient pressure and one at a high overburden pressure, and reduced permeability of the fractures up to four orders of magnitude. Recently, Willett et al. (2024) performed UICP at 60 °C on a fractured Marcellus shale core, obtaining a drop in permeability by three orders of magnitude. Using non-invasive tools, specifically nuclear magnetic resonance (NMR) and X-ray computed tomography (CT), results of this study revealed that calcite deposits bridged the gap of the fracture, creating a free-standing composite core. Another study reduced permeability in fractured shale by three to four orders of magnitude after UICP treatment was delivered at 60 °C and 70 °C (Hiebert 2019). Remarkably, when the biomineralized shale was pulled apart, new fractures were created in the rock rather than the original fracture now biomineralized. These findings suggest that UICP is capable of sealing fractures in shale rock. However, there still exists a need to investigate how a biomineral seal influences the mechanical properties of the composite UICP-shale core. The work presented here explores the tensile strength of UICP and fractured shale cores to better understand the mechanical properties of these composite materials.

1.3 Splitting tensile strength

Tensile strength is an important mechanical property in the characterization of rock failure that assesses the ductility of a material when it is pulled apart to the point of breakage (Dowling et al. 2019). Although direct tensile strength (DTS) methods, where a specimen is pulled apart, provide the most accurate and reliable tensile results, the tests are demanding and expensive to execute (ASTM 2008, 2016). The Brazilian indirect tensile strength (BITS) test is commonly used in lieu of a DTS test because it is inexpensive and easy to administer (ASTM 2016). Also referred to as the splitting tensile strength test, the BITS procedure applies an unconfined compressive load onto a cylindrical rock specimen until it breaks, or "splits" (Fig. 1).

Numerous studies have applied the BITS methods to intact shale discs to investigate the splitting tensile strength. Fracture patterns and failure modes are documented by Bisai and Chakraborty (2019). Li et al. (2017) found different tensile behavior between Eagle Ford and Mancos shale due to differences of mineralogy, water content, pre-existing fractures, and bedding-plane orientation and laminations. Particularly, tensile strength reduces up to 66% when pre-existing microfractures are present in the shale sample, as detected via X-ray CT scanning. Furthermore, shales with lower clay content (i.e., Eagle Ford) result in higher tensile strength. The anisotropic nature of shale has been thoroughly investigated using BITS testing to analyze the effects of bedding plane, lamination orientation, and/or loading orientation during time of testing (Gao et al. 2015; He and Afolagboye 2018; Hou et al. 2018; Mokhtari et al. 2014; Simpson et al. 2014; Wang et al. 2016). Iferobia et al. (2022) tested how thermally conditioned linear fracturing

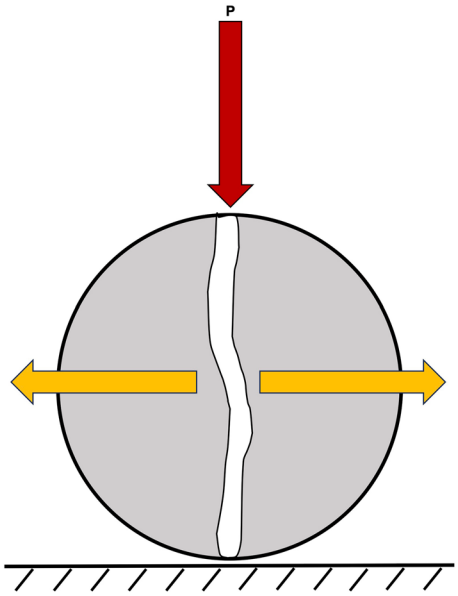

Fig. 1 Brazilian indirect tensile test schematic. An unconfined compressive load, P (vertical arrow), is applied to a disc-shaped specimen, inducing tensile stresses, until the specimen splits apart perpendicular to the applied compressive load (horizontal arrows)

fluid and elevated reservoir temperature conditions influence tensile strength of Eagle Ford and Wolfcamp shales. Overall, these studies conclude that shale type, temperature, bedding plane, water content, mineralogy, and pre-existing microfractures impact the splitting tensile strength of intact shale.

1.4 Overview

The research here is presented in two parts. Part one assesses the splitting tensile strength of intact Eagle Ford (EF) and Wolfcamp (WC) shale cores (5.08 cm long, 2.54 cm diameter) using a developed, modified BITS test method. The goal is to determine whether tensile strength is influenced by shale type and/or testing temperature conditions, specifically room temperature (RT) or 60 °C. Though 60 °C may not mimic actual subsurface temperatures of the shales used in this study, it was chosen because it approaches subsurface temperatures for shallow shale plays and promotes rapid ureolysis rates during UICP treatment of fractured cores. The yield strength of the intact shales to fracturing serves as a benchmark for understanding shale behavior after UICP treatment.

The objectives of part two are twofold: (1) seal shale fractures using UICP and (2) assess the splitting tensile strength of the resulting composite biomineralized shale. The first objective looks at two different methods to facilitate UICP in fractured shale cores: flow-through and immersion. The flow-through method, as outlined by Willett et al. (2024), uses the injection of UICP promoting solutions into a fractured shale core in a sequential pattern of microbes followed by urea and calcium-containing solutions to promote mineral precipitation. The immersion method directly applies a fracture treatment containing UICP promoting solutions and/or guar gum to fractured cores and places them in a batch reactor which was allowed to incubate over time. Guar gum is a polysaccharide and widely used as a viscosity thickener in the oil and gas industry to boost operation efficiency and reduce enhanced oil recovery costs (Barati and Liang 2014), making it a practical additive to include in UICP treatment for subsurface applications. After cores are sealed with UICP using either the flow-through or immersion treatment method, the second objective will use a modified BITS testing procedure to compare the resulting tensile strength of biomineralized cores. Cores sealed with the flow-through method will be compared to those sealed with the immersion method. In addition, a side-by-side comparison will be provided of the strength required to break cores in their intact state versus after they are fractured and sealed with UICP. Results from parts one and two of this study will guide future geomechanical modeling efforts.

2 Materials and methods

2.1 Shale cores

The first part of this study sourced 20 cores from commercially drilled outcroppings of two types of shale rock formations (Kocurek Industries, Inc., Caldwell, Texas). EF outcrops were sourced from four miles west of Comstock, Texas to Lozier Canyon. WC shale was sourced from surface outcrop in upper, mid-west New Mexico on the edge of the Permian Basin. Ten intact EF cores and 10 intact WC cores were subject to BITS testing and assessed for splitting tensile strength. All samples were cored parallel to the bedding plane with an

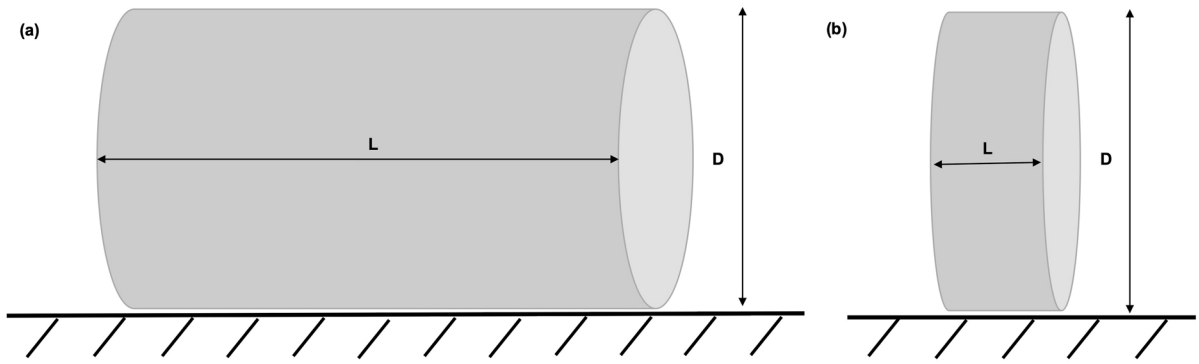

Fig. 2 **a** Core geometry used in this study with a 2.0 length to diameter ratio, **b** Disc-shaped specimen 0.5 length to diameter ratio, falling within ASTM standard geometry

approximate size of 5.08 cm (2 in) long by 2.54 cm (1 in) diameter, resulting in a length to diameter ratio of 2.0 (Fig. 2a). Although these 20 cores were not subject to UICP treatment, sample geometry was optimized for cores that underwent UICP treatment/experimentation in the second part of this study. This specific geometry called for a modification in BITS testing standards. Typically, disc-shaped samples adhere to a ratio of 0.2–0.75 for compliance with ASTM (Fig. 2b) (ASTM 2016). All cores were weighed, oven dried at 60 °C for a minimum of 24 h and weighed again before testing to ensure a constant weight and lack of moisture in pore spaces.

Two Marcellus and twenty-one EF shale cores underwent sealing experimentation in the second part of this study. Marcellus shale cores were provided by the National Energy Technology Laboratory (NETL) and sourced from a vertical well in Logan County, West Virginia and drilled perpendicular to the bedding plane. A description of the full core can be found in Crandall et al. (2019). EF shale cores were sourced from outcroppings of a large commercially drilled formation four miles west of Comstock, Texas out to Lozier Canyon (Kocurek Industries, Inc., Caldwell, Texas) and cored parallel to the bedding plane. All cores adhered to a geometry of 2.54 cm (1 in) diameter by 5.08 cm (2 in) length. An X-Ray diffraction (XRD) analysis detailing the mineralogical breakdown of both EF and Marcellus shales can be found in Willett et al. (2024). Prior to sealing

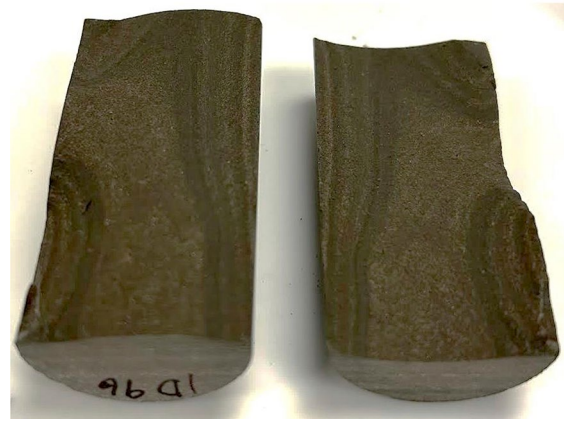

Fig. 3 Representative shale core (EF) fractured lengthwise with a single, heterogeneous fracture

experimentation, the modified BITS test procedure developed in part one was used to create a single, heterogeneous fracture through the length of each core (Fig. 3).

2.2 UICP: flow-through method

The flow-through sealing protocol followed those specified by Willett et al. (2024). In preparation for UICP treatment, a single, even layer of Granusil 2095 size (10/20) sand was applied to one half of the fractured shale, the other half was placed on top, and the two pieces were wrapped together with Teflon tape. Cores were housed in a braided PVC core holder connected to a syringe pump and placed inside an oven. Flow-through sealing experiments were conducted

at 60 °C. Prior to injections, cell preparation began when 100 mL of brain heart infusion (37 g/L), amended with 2% urea (20 g/L), was inoculated with 1 mL of thawed *S. pasteurii* (ATCC 11859) frozen stock culture, and placed in a 30 °C incubator at 150 rpm. After incubating for 24 h, the culture was transferred into yeast extract (YE) media and placed in a 30 °C incubator at 150 rpm. YE media was made using 15.5 g/L yeast extract, 35 g/L sodium chloride, 1 g/L ammonium chloride, and 20 g/L urea. After incubating for 16 h, 200 µL of culture was injected in triplicate into a Greiner Bio-One 96 flat bottom well plate, and the bacteria concentration was assessed using a Tecan Infinite F50 absorbance reader with a 600 nm filter, where the optical density at 600 nm (OD_{600}) was > 0.6. To promote mineral precipitation, a solution of urea and calcium (U + C) was made by combining 35 g/L sodium chloride, 1 g/L ammonium chloride, and 20 g/L urea; adjusting pH to 6.0–6.3; and subsequently adding 48 g/L calcium chloride dihydrate. Cell culturing and media preparation were influenced yet modified by methods proposed by Whiffin et al. (2007). *S. pasteurii* cells were injected into the core and given a 15-min stationary period, allowing cells to attach to the shale (although not confirmed), followed by an injection of U + C solution. Once the urea and calcium were inside the fracture, a 2-h stationary reaction period was allotted for biomineral promotion. Sequential treatment cycles of cells and U + C were injected into the fracture of the core until enough mineral formed to reduce the fracture permeability by three orders of magnitude (monitored by a pressure-flow relationship). Three cores (one EF and two Marcellus) were used with the flow through method.

2.3 UICP: immersion method

Four variations of the immersion method were tested on different fractures to explore the impact of each component on sealing (Fig. 4): (1) M, a control treatment of a calcium mineralizing media containing double concentrations of urea and calcium (2xCMM) with no cells or guar gum present (n = 1), (2) GM, a solution of guar gum mixed in 2xCMM (no cells) (n = 2), (3) CM, *S. pasteurii* cells suspended in 2xCMM (no guar gum) (n = 2), and (4) CGM, *S. pasteurii* cells suspended in a solution of guar gum mixed in 2xCMM (n = 5). All four treatments were tested at RT and 60 °C, each with the same number of "n" replicates. The immersion method treatment was performed on 20 EF cores. All mixtures utilized 2xCMM as a base fracture treatment fluid that consisted of 35 g/L sodium chloride, 1 g/L ammonium chloride, 3 g/L nutrient broth, and 40 g/L urea; a pH adjustment between 6.0 and 6.3; then adding 96 g/L calcium chloride dihydrate. The M treatment was simply 2xCMM fluid.

Fracture treatments that integrated guar gum were produced when 0.75 g guar gum was added to 50 mL of 2xCMM, creating a 1.5% guar solution. The intention of the GM treatment was to determine if the guar gum was capable of sealing fractures without the influence of mineral precipitation. Fracture treatments containing microbial cells incorporated an *S. pasteurii* culture into the 2xCMM base fluid. 200 mL of culture was spun down using a Thermo Scientific Sorvall Legend XTR Centrifuge at 2964xg for 10 min at 4 °C. The supernatant was removed, and bacterial pellets were resuspended in 50 mL of 2xCMM (OD_{600} > 1.8). The CGM treatment was the only condition to contain both *S. pasteurii* cells and guar gum in the 2xCMM base fluid.

Approximately 3 mL of fracture treatment was applied to the fractured faces of each core. After the M, GM, CM, or CGM fracture treatment was applied to the shale fracture, 0.5 g of Granusil 2095 size (10/20) sand (~ 1 mm in diameter) was evenly distributed in a single layer onto one half of the fractured core. The other half was placed on top, the two pieces were assembled, and ½ inch Teflon tape was wrapped around the center of the core to prevent displacement of the fractured halves. The cores and fracture treatment were then allotted a 30 min attachment period to allow cells, if present in the treatment, to attach to the shale and/or proppant before immersion in the batch reaction period. Cores designated for sealing at 60 °C were placed inside an oven preheated and conditioned to 60 °C for the duration of their attachment period. Cores selected for sealing at RT were left at RT for their attachment period.

Cores were then immersed in U + C (as prepared in flow-through methodology) for 48 h to promote mineral precipitation. Cores designated for sealing at 60 °C were placed inside an oven preheated to 60 °C for the duration of their 48-h batch reaction period. Those at RT were left at RT for their batch reaction period. After the batch reaction period, cores were

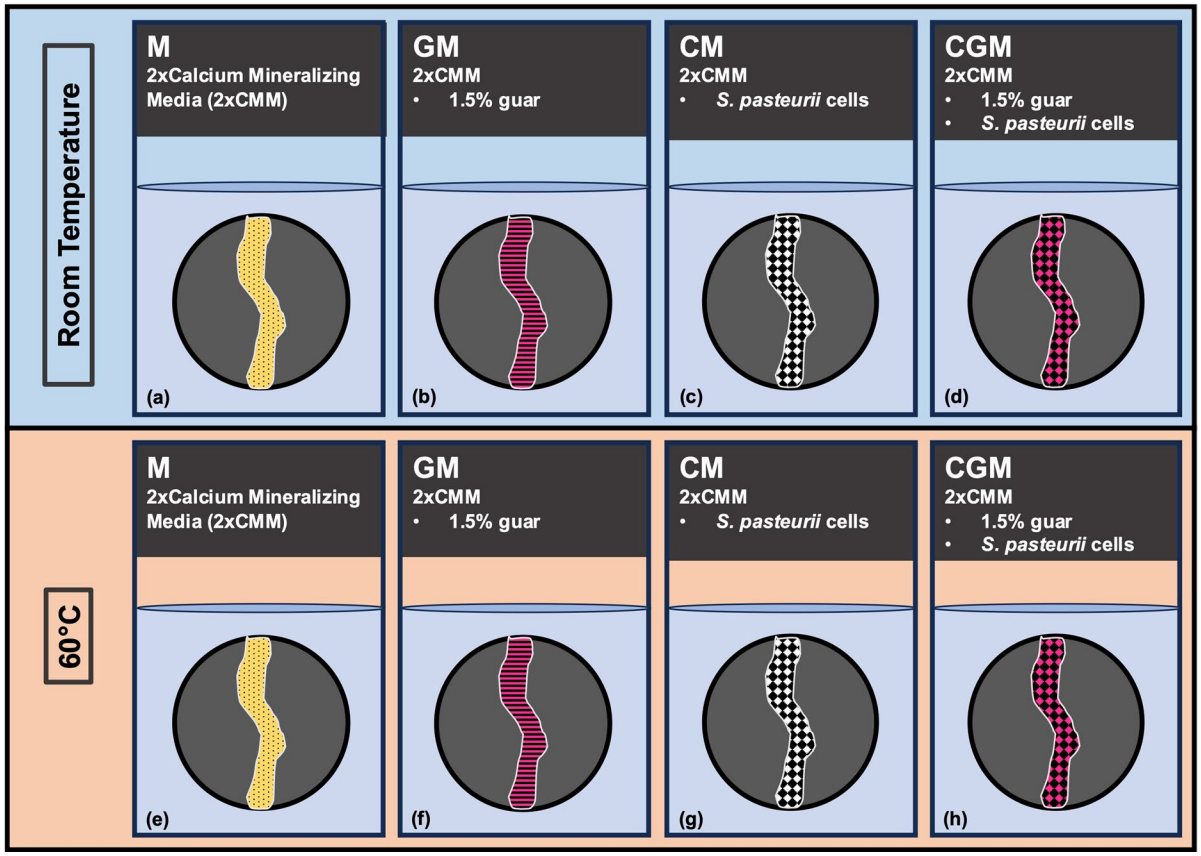

Fig. 4 Four fracture treatments investigated with the immersion method. All conditions used 2xCMM (calcium mineralizing media (CMM) with double the concentration of urea and calcium chloride dihydrate) as a base fracture treatment. **a** and **e** The M treatments assessed 2xCMM's ability to seal fractures (n = 1). **b** and **f** The GM treatments incorporated a 1.5% guar gum concentration into 2xCMM to enhance viscosity and determine if guar gum influences core sealing (n = 2). **c** and **g** The CM treatments integrated S. pasteurii cells (measured optical density at 600 nm (OD_{600}) > 1.8) into 2xCMM fluid to promote mineral precipitation inside the fracture (n = 2). **d** and **h** The CGM treatments combined 1.5% guar gum and S. pasteurii cells (OD_{600} > 1.8) into the 2xCMM (n = 5). All four treatments were tested at RT and 60 °C, each with the same number of "n" replicates

removed from their beakers and placed in a 40 °C incubator to dry for five days. The core mass was weighed over the five-day period until mass stabilized. Once dry, the Teflon tape was removed, and cores were inspected for sealing. Figure 5 depicts the immersion method steps. Sealing was designated successful when the fracture treatment attached the two shale halves to one another without the aid of tape.

2.4 Splitting tensile strength core testing

A modified BITS testing procedure was used to evaluate the splitting tensile strength of intact and sealed cores. Tests were administered on an MTS Criterion Model 43 test frame enclosed in an environmental chamber that allowed testing at elevated temperatures. Testing was completed with a 30 kN load cell and the cutoff load was set to 28 kN. Curved loading platens were designed to accommodate the geometry of the cores in this study and fabricated to connect with the test frame. Splitting tensile strength was calculated using Eq. 2:

$$\sigma_t = 1.272P/\pi tD \quad (2)$$

where σ_t is the splitting tensile strength (MPa or psi), 1.272 is the coefficient when curved platens are used, P is the maximum applied load indicated by the

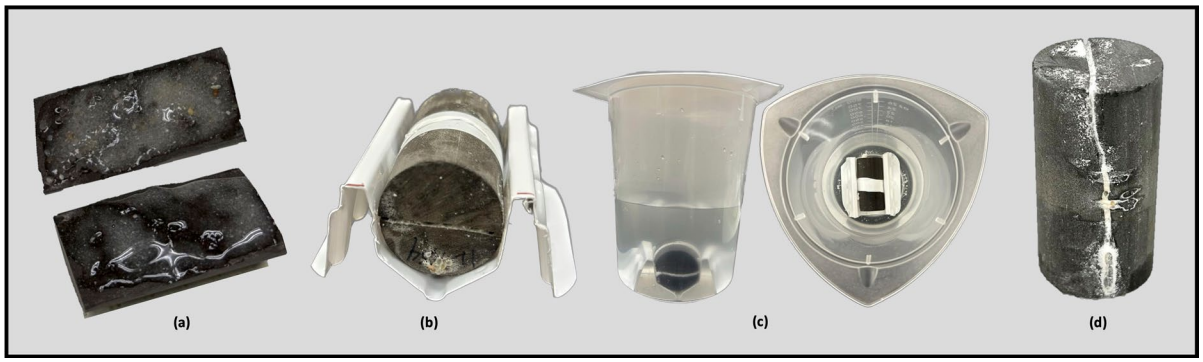

Fig. 5 Immersion method steps. **a** Apply ~ 3 mL fracture treatment (i.e., M, GM, CM, or CGM) to fracture faces and place 0.5 g proppant. **b** Assemble cores halves together and wrap 1/2-inch Teflon tape around center of core. Let sit at the designated temperature; RT or 60 °C; for 30 min. **c** Immerse into U + C, at designated temperature, for 48 h. **d** Remove from immersion after 48 h and place in 40 °C incubator to dry for five days. After five days, take out of incubator, remove Teflon tape, and inspect for sealing

testing machine (N or lbf), t is the thickness of the specimen (mm or in), and D is the diameter of the specimen (mm or in) (ASTM 2016). Equation 2 is specific to BITS tests utilizing curved loading platens, as indicated by the coefficient 1.272. Curved loading platens are used on the cores in this study to reduce the stress concentration at the loading points (ASTM 2016; Mellor and Hawkes 1971). A picture of these platens is shown in the results (Fig. 17a).

Of the 20 intact cores evaluated in part one, 10 cores (five EF and five WC) were tested at RT and 10 cores (five EF and five WC) were tested at 60 °C. For the 60 °C testing, the environmental chamber surrounding the MTS testing system was pre-heated to temperature (60 °C) and the cores were placed inside the heated chamber prior to testing for a 3-h equilibration period to promote homogeneous heat distribution throughout the samples (not confirmed). The intact cores for both parts one and two were cored parallel to the bedding plane. For part one testing, the cores were oriented such that the intersection angle was 0° between the bedding plane and loading direction (Fig. 6a). In part two of this study, the 21 originally intact EF cores used for sealing experimentation were fractured at RT using the above BITS methodology to create a single, heterogeneous fracture

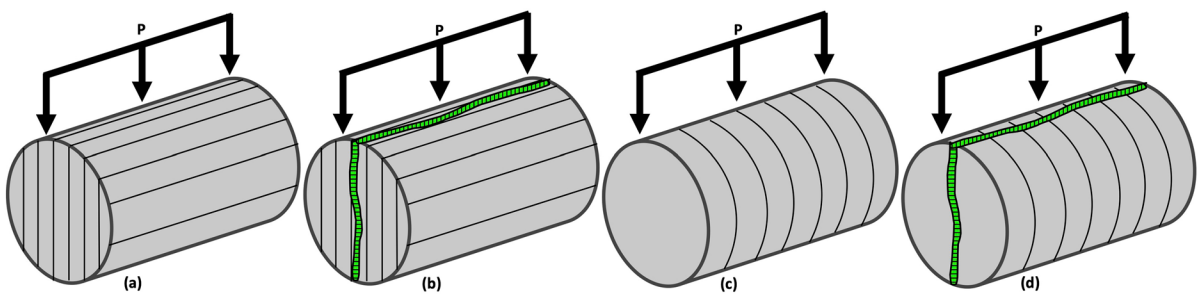

Fig. 6 Loading direction (black arrows) relative to the core bedding planes (black lines through cores) and relative to the sealed fractures (green-striped lines). Depicted bedding planes are representative and were not quantified. P indicates the unconfined compressive load applied to the shale core to induce tensile stresses. **a** Samples cored parallel to the bedding plane with loading direction relative to the bedding plane at an intersection angle of 0°. **b** Fractured and sealed samples cored parallel to the bedding plane, with a 0° intersection angle between the loading direction relative to the bedding plane and to the sealed fracture. **c** The applied load crossed the bedding plane for intact samples cored perpendicular to the bedding plane. **d** Fractured and sealed samples cored perpendicular to the bedding plane, the applied load crossed the bedding plane but had a 0° intersection angle between the loading direction and sealed fracture

spanning the length of the core where the loading direction relative to bedding plane mimicked that in part one (Fig. 6a). Marcellus cores (cored perpendicular to the bedding plane and fractured by NETL) experienced an applied load that crossed the bedding plane (Fig. 6c). For successfully sealed cores, composite core tensile strength was evaluated at the temperature used to seal the core, either RT or 60 °C (i.e., cores sealed at 60 °C were BITS tested at 60 °C). As before, cores tested at 60 °C were placed inside the pre-heated environmental chamber for a 3-h equilibration period prior to testing. Sealed cores were positioned such that the intersection angle between the loading direction and the sealed fracture was as close as possible to 0° (Fig. 6b, d). Some sealed fractures were less planar than others, as depicted in the results (Fig. 12), which may have caused variability in the loading angle between cores.

2.5 Statistical analysis

R version 4.2.1 (R Core Team 2022) was used to analyze data obtained from the intact cores in part one. A two-sample t-test investigated the difference in average tensile strength values for EF and WC shale cores tested at RT and 60 °C. Two separate two-sample t-tests were run to investigate the effect temperature had on EF and WC cores independently, ultimately to determine if there was a statistical difference between cores tested at RT versus cores tested at 60 °C. Another two-sample t-test compared the averages of all EF samples versus all WC samples to determine if there was a statistical difference in tensile strength of one shale type compared to the other.

3 Results and discussion

3.1 Splitting tensile strength: intact cores

Four intact core sample groups, each containing five replicates (n = 5), were evaluated for splitting tensile strength. A value of five replicates was chosen to account for statistical variation in shale. Group one contained samples of EF shale tested at room temperature resulting in an average tensile strength of 7.22 ± 0.55 MPa. EF samples in the second group were tested at 60 °C resulting in an average tensile strength of 6.02 ± 0.55 MPa. The third group consisted of WC cores tested at room temperature where the average tensile strength was 6.07 ± 1.35 MPa.

Table 1 Average tensile strength (MPa) per intact shale core sample group

Shale type: temperature	Ave tensile strength (MPa)
EF: RT	7.22 ± 0.55
EF: 60 °C	6.02 ± 0.55
WC: RT	6.07 ± 1.35
WC: 60 °C	5.46 ± 2.44

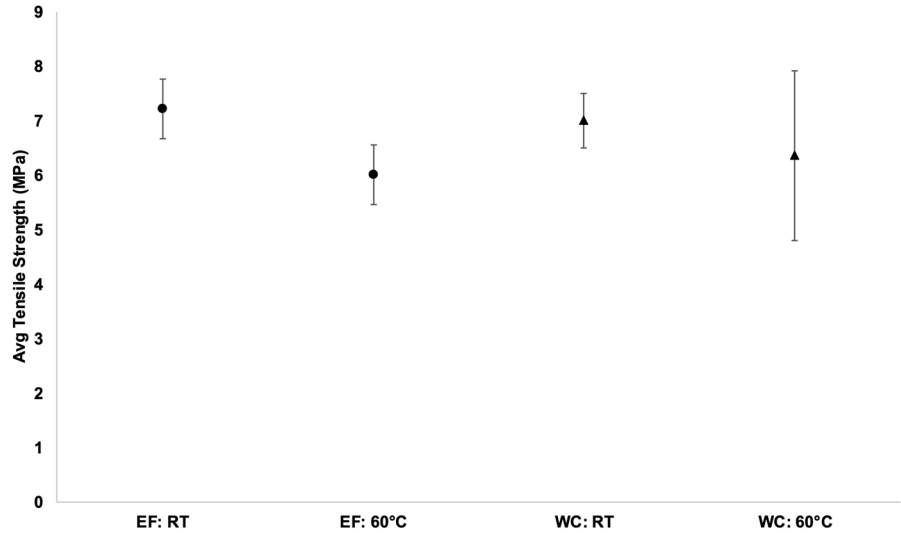

Fig. 7 Average tensile strength (MPa) and standard deviation for each type of shale and temperature combination. Each sample group contains five replicates. EF shale is represented by circles and WC shale is represented by triangles

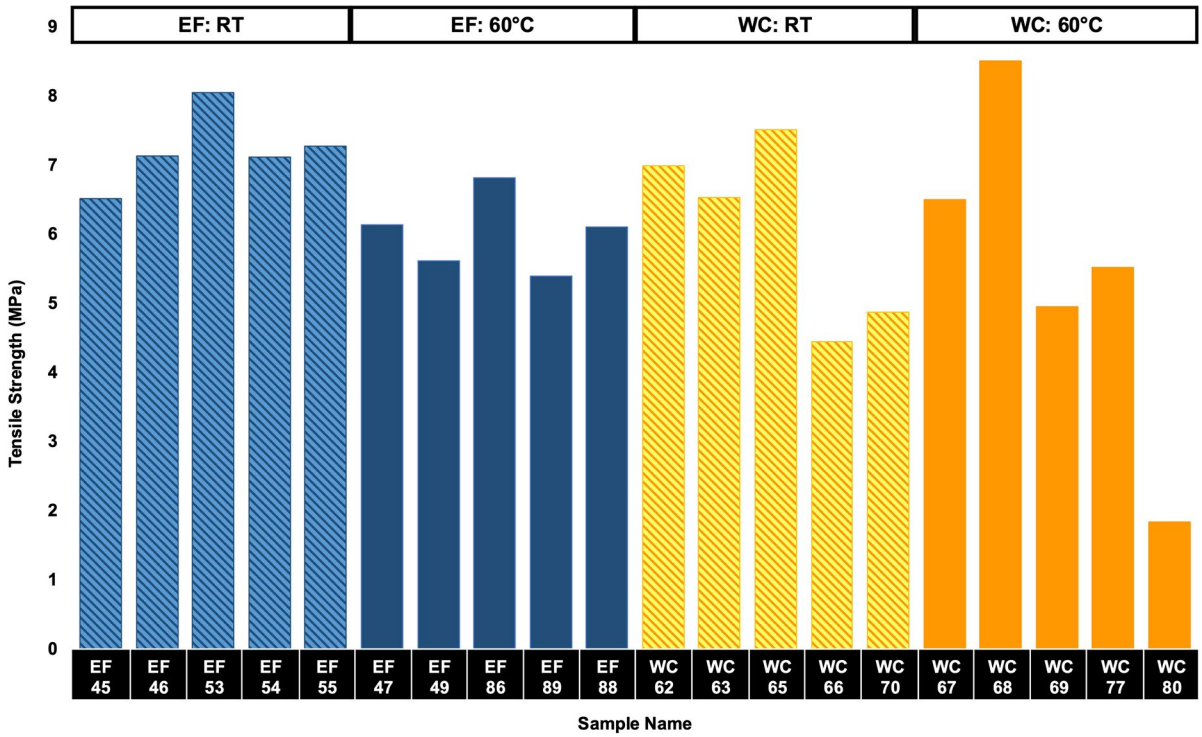

Fig. 8 Tensile strength (MPa) comparison of 20 intact shale samples tested using BITS. Blue bars represent EF samples and yellow bars represent WC samples. Darker bars indicate samples tested at 60 °C and lighter bars with dark diagonal lines indicate samples tested at RT

Group four tested WC samples at 60 °C producing an average tensile strength of 5.46 ± 2.44 MPa. Figure 7 and Table 1 summarize and compare results of average tensile strength for each sample group; additionally, Fig. 8 lists the individual sample names for the tests and provides the tensile strength of each intact core tested in part one.

Within both temperature conditions, WC samples demonstrated higher tensile strength variability compared to EF samples. Notably, WC cores tested at 60 °C exhibited the highest (WC-68 at 8.51 MPa) and lowest (WC-80 at 1.83 MPa) strengths of any intact core tested. The lowest tensile strength was believed to be caused by the existence of visible fractures in the core prior to testing (Fig. 9b). Cores WC-66, 70, 77, and 80 all contained visible fractures spanning some aspect of the core. Although these cores contained initial fractures, they remained intact, free-standing cylindrical cores maintaining their 5.08 cm length by 2.54 cm diameter geometry. Cores WC-66 and WC-70 produced the lowest tensile strength values for any core tested at RT. At 60 °C, although WC-80 resulted in the lowest overall tensile strength, WC-77 generated only the third lowest tensile strength in this sample group which was greater than a core with no visible fracture prior to testing (WC-69). Figure 9 provides evidence of visible fractures in cores WC-66 and WC-80, tested at RT and 60 °C, respectively. The variability in tensile strength and existence of fractures could be the result of sample coring procedures, geological processes, and/or the general anisotropic nature of shale. No EF cores contained visible fractures prior to testing. Additionally, no cores in this study were subject to preliminary CT scans, so the existence of non-visible, internal fractures was unknown. Li et al. (2017) found that the tensile strength of shale can be reduced up to 66% when pre-existing micro-fractures are detected and that bedding plane/laminations significantly impacted EF shale tensile strength values. Although WC shale was not tested in their study, the work presented here observed that cores with existing fractures, found specifically in WC groups, contributed to the greater standard deviation associated with average tensile

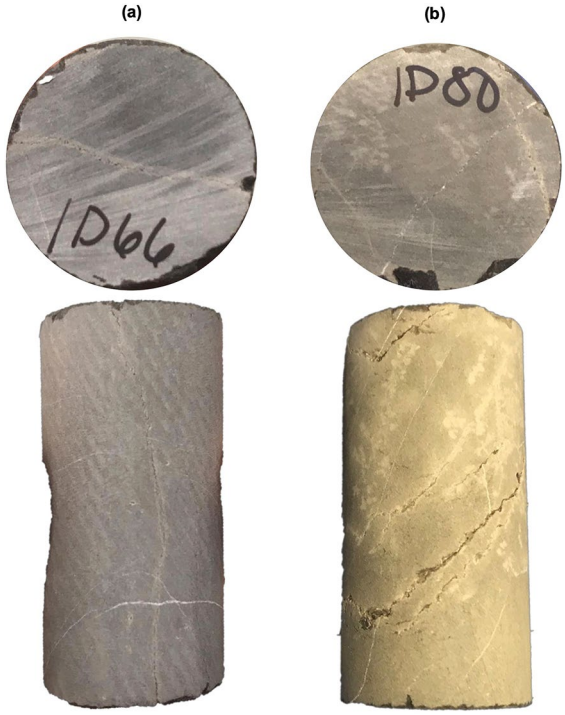

Fig. 9 Representative WC samples with visible fractures pre-BITS testing. **a** WC-66 tested at RT contained a fracture along the length of core. **b** WC-80 tested at 60 °C with a radial fracture recorded the lowest tensile strength value (1.83 MPa) out of all cores tested in part one

strength for the sample group. It is likely that WC cores with pre-existing fractures lowered the average tensile strength value at the 60 °C temperature condition. However, because both RT and 60 °C temperature conditions had two out of five WC cores with pre-existing fractures as well as the low sample size (n = 5), they remained in the analysis.

Again, all sample groups demonstrated variations in tensile strength between the five replicates. However, the EF cores expressed less tensile strength variation between replicates than WC cores (Fig. 8). The resulting standard deviation values (Fig. 7 and Table 1) were appropriately lower for EF sample groups and higher for WC sample groups, further suggesting the difference in variability between shale types. Although trends were observed in the data, the statistical analysis indicated the difference in mean tensile strength between shale types (without considering temperature condition) was not significantly different (two-sided p-value = 0.2064). The statistical model was verified to meet assumptions of constant variance and normality.

Results of this study suggest a decrease in average tensile strength when temperature was increased to 60 °C for both EF and WC (Table 1). When tested at 60 °C compared to RT, the average tensile strength for EF and WC shales was reduced approximately 17% and 10%, respectively. The hypothesis that RT sample groups would exhibit a higher tensile strength versus sample groups at 60 °C was statistically confirmed between EF temperature conditions (one-sided p-value = 0.0043). However, the observed trends were challenged between WC sample groups when analysis showed no significant difference in mean tensile strength between temperature conditions (one-sided p-value = 0.3198). Furthermore, assumptions of constant variance and normality were verified in the statistical models. Strikingly, the observations and findings associated with temperature and strength oppose the findings of other research where shale tensile strength increased as temperatures increased from RT to near 100 °C. Using BITS methods, Vishal et al. (2022) tested shale at room temperature, 50 °C, 100 °C, 200 °C, and 400 °C to determine the temperature effect on tensile strength. They concluded that there was a significant increase in average strength up to 100 °C but strength decreased when temperatures exceeded 100 °C. They hypothesize that the increase in values up to 100 °C may be from removal of water present in the rock. However, their BITS procedure was not administered at temperature; samples were heated to temperature for three hours then allowed to cool to RT before testing. Similarly, Iferobia et al. (2022) exposed samples of EF and WC shale to 90 °C for 5 and 20 days and discovered that average tensile strength increased compared to samples tested at RT. They also exposed samples of EF and WC shale to 220 °C for five days and found a decrease in average tensile strength compared to samples tested at RT.

3.2 Splitting tensile strength: fractured and sealed

Prior to sealing, BITS methods were used to create a single heterogeneous fracture along the length (5.08 cm) of the intact shale cores used in sealing experimentation. The average compressive load applied to the intact EF shale cores (n = 20) was 17.59 ± 2.26 kN, resulting in a splitting tensile strength of 5.52 ± 0.71 MPa. Loads applied to the

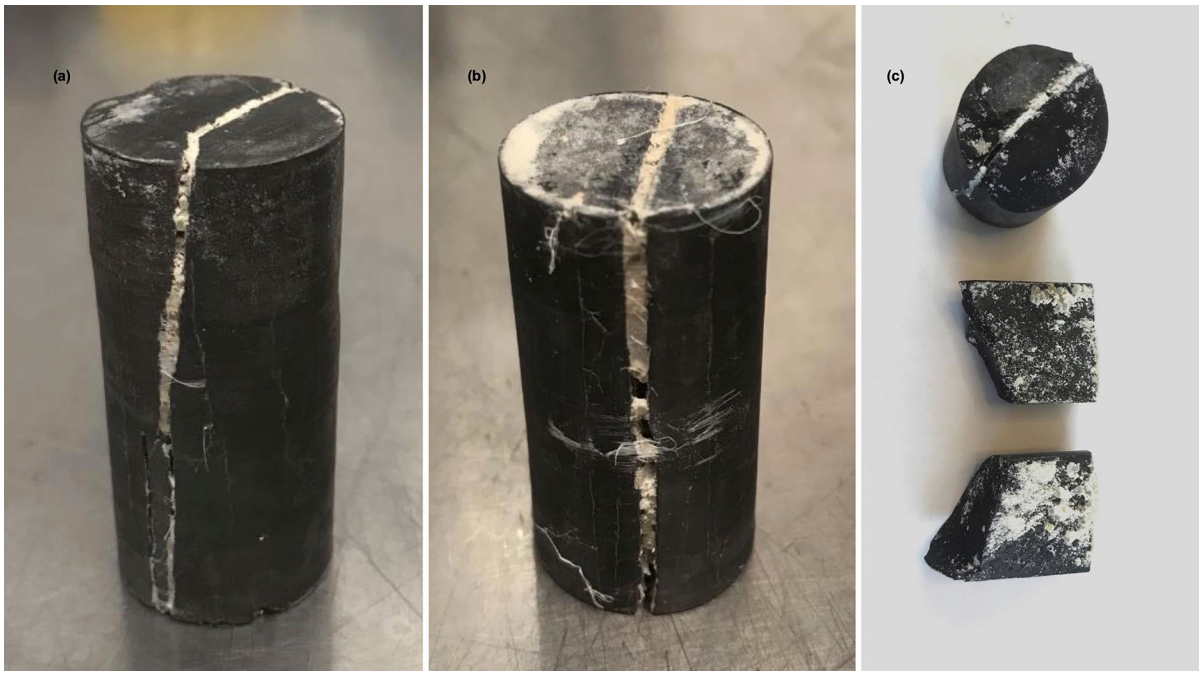

Fig. 10 Shale cores sealed with UICP technology using the flow-through method. **a** Marcellus core, M-29. **b** Marcellus core, M-32. **c** EF core, EF-48, which suffered a secondary fracture during UICP treatment while inside the core holder, causing it to split into two approximate 1-inch halves along its length. The half of the core closest to the fluid influent sealed with biomineralization and the half near the effluent did not seal. Fully sealed and partially sealed cores were tested for mechanical strength

Marcellus cores were not measured by collaborators at NETL.

The flow-through method sealed three shale cores (two Marcellus and one EF) with biomineralization (Fig. 10). Each core received between 20 and 30 injections of UICP treatment until permeability in the fracture reduced by three orders of magnitude. Once removed from the flow-through reactor, cores that were once two pieces of shale were connected and held together with biomineralization, similar to what has been seen in previous UICP-shale research (Cunningham et al. 2015; Hiebert 2019). Both Marcellus cores (M-29 and M-32) were sealed along their entire length, creating a 5.08 cm long composite core (Fig. 10a, b). However, the EF core (EF-48), suffered a secondary fracture during UICP treatment while inside the core holder, likely due to hose clamps applying an overburden pressure to the core, causing it to split axially into two halves of approximately equal size, around 1 inch each (Fig. 10c). The half of the core closest to the influent of fluids was successfully held together (sealed) with biomineralization whereas the half near the effluent was not connected. The approximate 1-inch sealed half of EF-48, along with M-29 and M-32, were tested for mechanical strength. Flow-through cores experienced multiple breaks before experiencing a maximum failure event. Table 2 displays the maximum compressive load as well as the calculated splitting tensile strength that each core experienced during their respective BITS test.

Table 2 Maximum compressive load (kN) applied to cores sealed with the flow-through method and the calculated splitting tensile strength (MPa) results

Core ID	Compressive load (kN)	Splitting tensile strength (MPa)
M-29	5.26	1.71
M-32	9.82	3.20
EF-48*	13.71	4.46
Average	9.60 ± 4.23	3.12 ± 1.38

*EF-48 broke axially into two halves during UICIP treatment and only the half that sealed was mechanically tested

The immersion method sealed fourteen of the twenty EF shale cores, with success being found in treatments utilizing guar gum. Here, successful sealing was defined when the applied fracture treatment allowed cores that were once two pieces to become one composite free-standing core. Cores treated with only CM (*S. pasteurii* culture in 2xCMM base fluid) and M (2xCMM base fluid) did not seal under either temperature condition (Fig. 11). Cores that did not seal (six total) were not mechanically tested. A tensile strength of 0 MPa was assumed for unsealed cores.

The GM (guar gum in 2xCMM base fluid) and CGM (*S. pasteurii* culture and guar gum in 2xCMM base fluid) fracture treatments experienced 100% success in sealing cores (14 total) under both temperature conditions (Fig. 12). These results demonstrated that guar gum can positively influence core sealing under batch conditions. Although approximately the same quantity of microbes was applied to cores under the CM and CGM fracture treatments, the CGM cores likely exhibited sealing success because the microbial cells were suspended in a higher viscosity guar gum fluid, allowing microbes to remain inside the fracture for the sealing process. When CM was applied as a fracture treatment, the treatment had difficulty staying inside the fracture during the attachment period preceding core immersion. Furthermore, once CM-treated cores were immersed in U + C, it is likely cells diffused out of the fracture, which would result in less mineralization. Figure 11b shows evidence of mineral precipitation attaching pieces of proppant to each other as well as to the shale rock; however, mineral precipitation was not sufficient to attach the shale halves to one another. All sealed cores were mechanically tested using a modified BITS method.

Cores under the GM fracture treatment demonstrated two distinct results. Cores at RT conditions (EF-109 and EF-119) maintained fracture cohesion with guar gum during and after tensile testing (Fig. 13a), unlike those sealed and tested at 60 °C (EF-91 and EF-99) which experienced fracture treatment failure after testing (Fig. 13b). The load–displacement curves for GM treated cores (Fig. 14) indicate distinct failure episodes occurring between 20 and 27 kN for most of these cores. These results suggest further research is necessary to fully determine the impact guar gum plays in fracture sealing and as an additive to UICP technology. Due to a small sample size (n = 2 per temperature condition) it is difficult to draw distinct conclusions and additional experimentation should be considered.

Multiple breaks were observed in cores sealed with UICP (CGM treatments) using the immersion method (Table 3 and Fig. 15). Table 3 reports the significant failure episodes for sealed cores treated with guar gum, cells, and UICP promoting solutions (CGM). Cores using this fracture treatment

Fig. 11 Representative unsealed cores from the M and CM fracture treatments. **a** EF-102 used the M fracture treatment where no microbial cells or guar gum was used, resulting in no mineral precipitation and no sealed cores. **b** EF-108 used the CM fracture treatment, there is evidence of mineral formation, but no cores were able to seal using this treatment

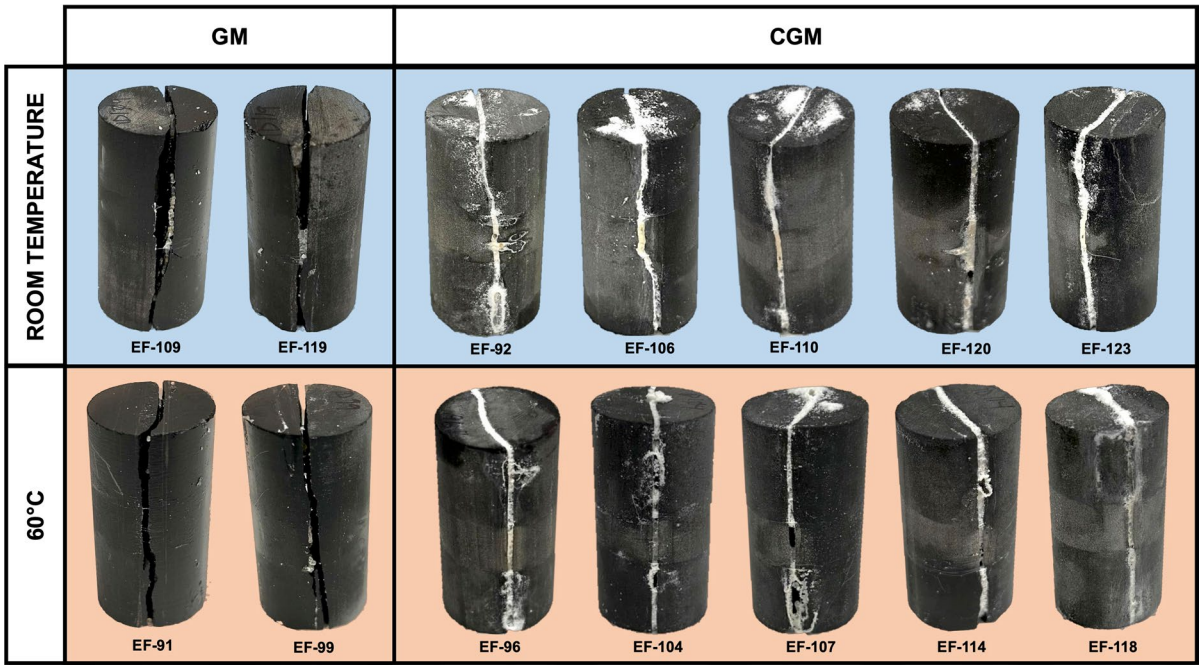

Fig. 12 Cores sealed using the immersion method. Four cores (two at RT and two at 60 °C) were sealed using the GM fracture treatment that contained guar gum and UICP promoting fluids (no cells). Ten cores (five at RT and five at 60 °C) were sealed using the CGM fracture treatment that contained microbial cells, guar gum, and UICP promoting fluids

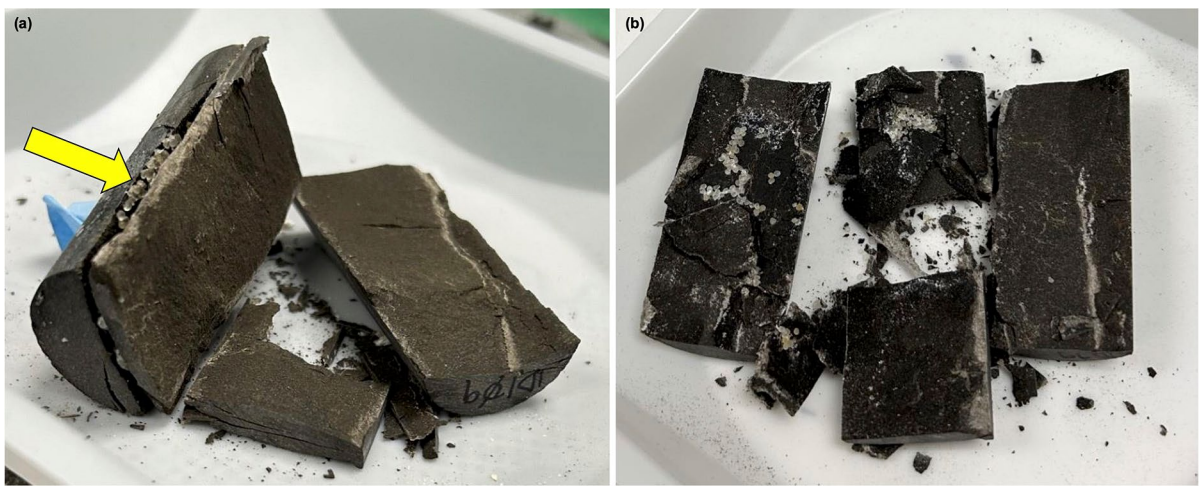

Fig. 13 Representative cores sealed using the immersion method and GM fracture treatment. **a** EF-109 sealed at RT, the arrow points to the original fracture maintaining cohesion with guar gum. **b** EF-99 sealed at 60 °C where the guar gum seal failed

experienced their first indication of failure at an average compressive load of 0.66 ± 0.19 kN (average splitting tensile strength $= 0.21 \pm 0.06$ MPa) and 0.55 ± 0.07 kN (average splitting tensile strength $= 0.17 \pm 0.02$ MPa) when tested at RT and 60 °C, respectively (Table 3 and Fig. 15). Out of the 10 total composite cores, three (EF 110 and EF-123 at RT and EF-96 at 60 °C) experienced failure in the mineralized fracture at the first indication of failure, at a load < 1 kN, when the testing apparatus detected

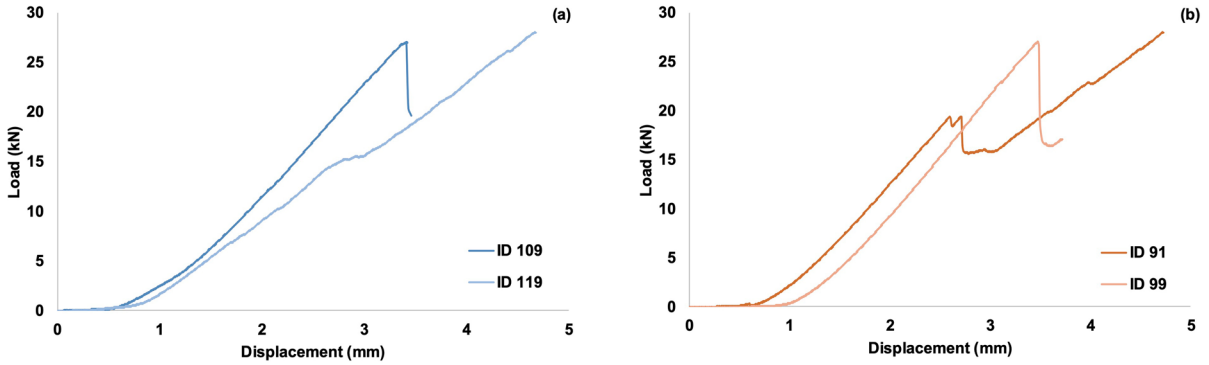

Fig. 14 GM fracture treatment load (kN) vs displacement (mm) curves. **a** RT cores **b** 60 °C cores

Table 3 Significant failure episodes for cores sealed with the immersion method using the CGM fracture treatment as determined with BITS testing methods

Failure for each episode is reported in compressive load, C (kN), and the calculated splitting tensile strength, σ_t (MPa), using Eq. 2

T	Core ID	1st Failure		2nd Failure		3rd Failure		4th Failure		Load Cell Limit	
		C (kN)	σ_t (MPa)	C	σ_t	C	σ_t	C	σ_t	C	σ_t
RoomTemp	EF-92	0.97	0.31	17.58	5.52	23.53	7.38	–	–	28.03	8.80
	EF-106	0.66	0.21	6.67	2.09	–	–	–	–	–	–
	EF-110	0.63	0.20	–	–	–	–	–	–	–	–
	EF-120	0.46	0.15	13.38	4.20	–	–	–	–	28.04	8.80
	EF-123	0.56	0.17	–	–	–	–	–	–	–	–
60 °C	EF-96	0.48	0.15	–	–	–	–	–	–	–	–
	EF-104	0.49	0.15	14.63	4.59	24.12	7.57	–	–	28.05	8.80
	EF-107	0.59	0.19	0.84	0.26	22.38	7.02	25.31	7.94	28.03	8.80
	EF-114	0.52	0.16	16.58	5.20	–	–	–	–	28.06	8.80
	EF-118	0.64	0.20	19.91	6.25	–	–	–	–	28.02	8.80

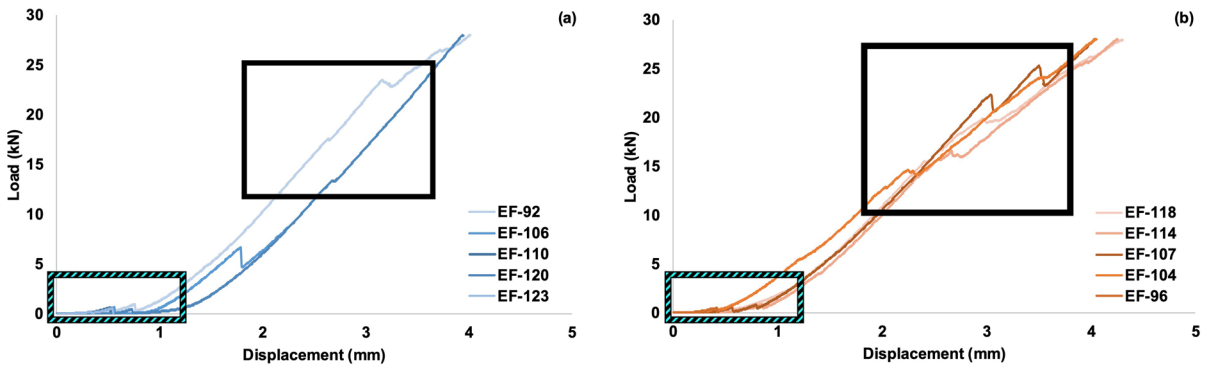

Fig. 15 CGM fracture treatment load (kN) vs. displacement (mm) curves. The small, dashed box highlights the first indication of failure (< 1 kN). The large black box highlights the second + failure episodes. **a** RT **b** 60 °C cores

failure and ended the test abruptly. When removed from the testing apparatus, these cores were split apart at the mineralized fracture. Although the other seven composite cores also experienced a break at a load < 1 kN, complete capacity was not lost and the test was able to continue, incurring further breakage.

At 60 °C, cores EF-104, EF-107, EF-114, and EF-118 suffered a significant second (third or fourth) failure episode in the range of 15–25 kN (Table 3 and Fig. 15b). This was also seen at RT in EF-92 (Fig. 15a). However, EF-106 and EF-120 did not show a similar trend. EF-106 experienced a second break much sooner at 6.67 kN and the test ended when the testing apparatus detected this break. EF-120 experienced a minor failure episode at 13.38 kN but the test ended only when the load cell reached its load limit of 28 kN. Both cores broke at the mineralized fracture. Notably, four cores at 60 °C and two cores at RT experienced a test that ended when the load cell reached its limit cutoff load of 28 kN. Upon removing cores from the apparatus, visible fractures in the shale rock matrix were evident. Of the four 60 °C cores, three (EF-104, EF-114, and EF-118) maintained mineral cohesion and exhibited new fractures in the surrounding shale rock; as did one of the RT cores (EF-92). Mineral cohesion means that the biomineral sealing the fracture together did not experience enough failure to break apart. These results may indicate that the load cell used in the testing apparatus was not strong enough to test the full capacity of a biomineralized seal.

Regardless of sealing method, results on how and where each biomineralized core broke were unpredictable (Figs. 16 and 17). The load (kN) versus displacement (mm) curves for cores sealed with the flow-through method compared to those sealed with the immersion method show visual differences in how the composite cores reacted to BITS testing (Fig. 16). Figure 16a showcases the variety of failure episodes experienced by cores sealed with the flow-through method (n = 3). The maximum load incurred by a flow-through core was 13.71 kN (tensile strength = 4.46 MPa) as seen by EF-48. In contrast, cores sealed with the immersion method exhibited fewer failure episodes (one–four episodes per core) and failure trends were similar between temperature conditions (Fig. 16b, c). The solid and dashed red lines, respectively, represent the average applied load and standard deviation (17.59 ± 2.26 kN, average splitting tensile strength = 5.21 ± 0.71 MPa) achieved when a single, heterogeneous fracture was created in the EF cores (n = 20) used in part two. Notably, this average load falls within the range of the second, third, or fourth failure episodes some composite cores

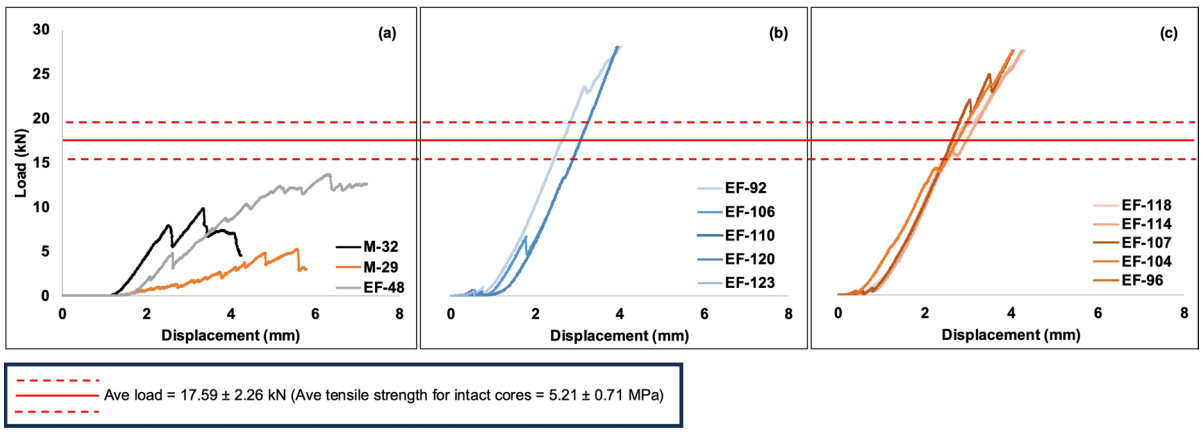

Fig. 16 Load (kN) vs. displacement (mm) curves for all cores sealed with UICP. The solid red line indicates the average load (kN) required to break the intact EF shale cores (n = 20), used in part two, prior to sealing with the immersion method and the dashed red lines indicate the standard deviation associated with the average. **a** Curves for cores sealed with the flow-through method at 60 °C. **b** Curves for cores sealed with the immersion method at RT. **c** Curves for cores sealed with the immersion method at 60 °C. Cores sealed with the immersion method utilized cells, guar gum, and UICP promoting solutions in the CGM fracture treatment

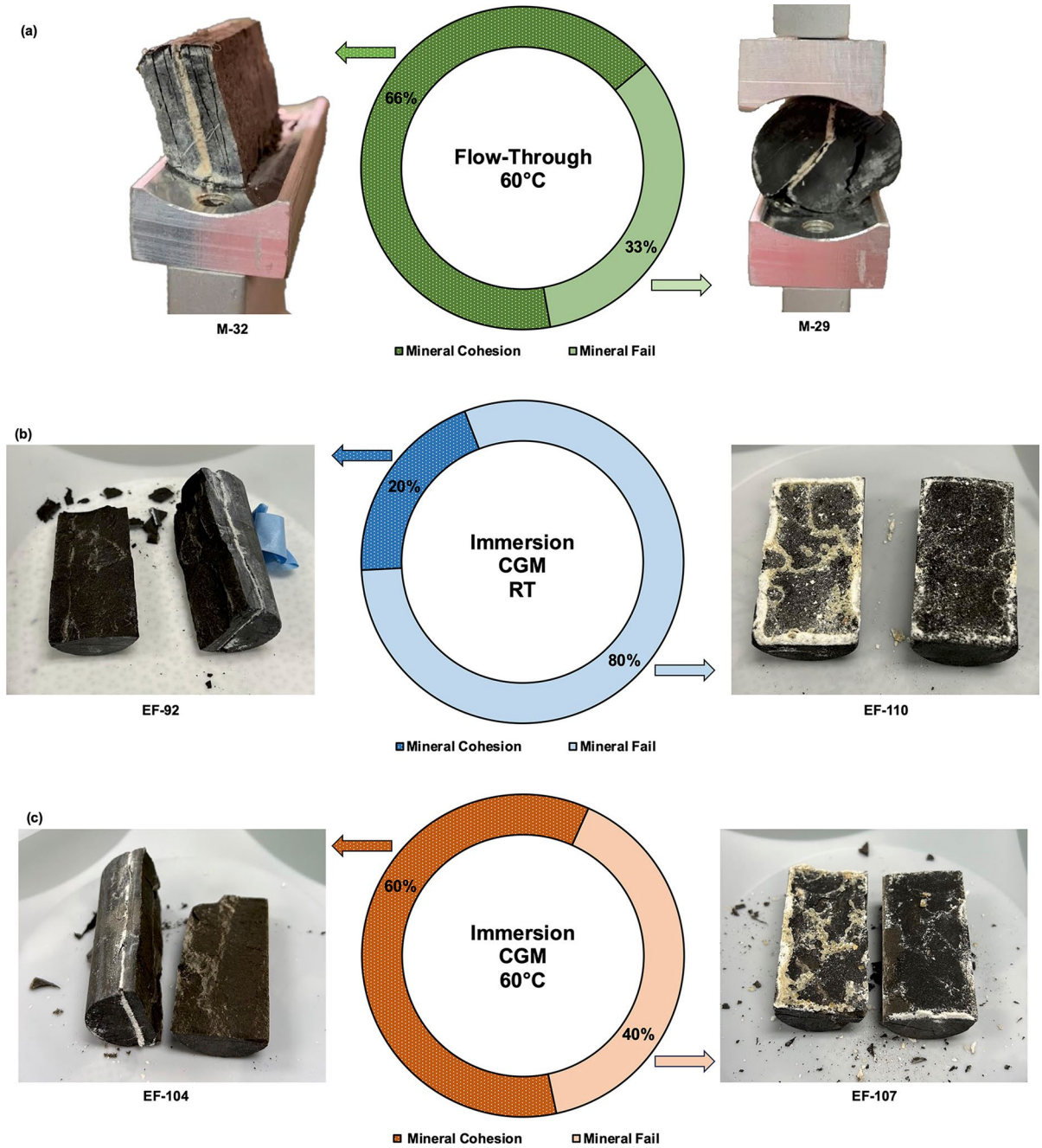

Fig. 17 Percentage of mineral cohesion (dark color) versus mineral failure (light color) post BITS testing for cores sealed with UICP. **a** The flow-through method at 60 °C. Three cores were sealed and tested at 60 °C, where one (M-29) experienced mineral failure during testing and two maintained mineral cohesion during and after testing, like the representative core M-32. **b** The immersion method at RT. Five cores were sealed and tested at RT, where four experienced mineral failure during testing, like representative core EF-110, and one (EF-92) maintained mineral cohesion during and after testing. **c** The immersion method at 60 °C. Five cores were sealed and tested at 60 °C, where two experienced mineral failure during testing, like representative core EF-107, and three maintained mineral cohesion during and after testing, like the representative core EF-104

experienced (15–25 kN), suggesting that the shale rock was likely breaking during these episodes.

Differences in the failure behavior may be attributed to the UICP sealing methods. Cores sealed with the flow-through method were subjected to more handling in which they were saturated in UICP promoting fluids at 60 °C for seven to ten days, received 20–30 bacterial applications, experienced overburden pressure from the core holder design, and were subject to NMR and CT analysis before and after UICP treatment. The authors hypothesize that these more rigorous methods may have influenced the shale rock matrix but acknowledge that more experimentation needs to be done to draw any conclusions. Comparatively, cores sealed with biomineral using the immersion method were saturated in UICP promoting fluids for two days (five cores at RT and five cores at 60 °C), received one bacterial application, and experienced no overburden pressure during the immersion process; however, they did have guar gum incorporated into UICP promoting fluids. Nevertheless, the unpredictability of core breakage remains, making it difficult to draw comparisons between UICP treatment methodologies. In some cases, the mineralized fracture remained intact showing more cohesion than the surrounding shale rock, similar to what was seen in the work by Heibert (2019). In other cases, the biomineralized fracture experienced mineral failure and broke open from an insufficient seal. Of the three cores sealed with the flow-through method, two experienced mineral cohesion and one mineralized fracture split apart during the BITS test (Fig. 17a). Cores sealed at 60 °C using the cells and guar fracture treatment had better mineral cohesion success than those at RT. Overall, 60% of 60 °C cores (n = 5) experienced mineral cohesion compared to only 20% at RT (n = 5) (Fig. 17b, c).

While it is difficult to predict how the cores would break, several causes of heterogeneity in the composite UICP-shale cores could be the reason. The authors hypothesize changes in the shale rock matrix due to UICP promoting fluid exposure, however this is not yet confirmed. The Iferobioa et al. (2022) study (that investigated how temperature affected the splitting tensile strength of EF and WC shales) further explored how tensile strength and percentage of sample mass increase was impacted for EF and WC shale samples that were saturated in thermally conditioned (90 °C) linear fracturing fluid of various polymeric concentrations. Linear fracturing fluid is used in subsurface applications to increase viscosity of aqueous solutions for the enhancement of proppant suspensibility, flowback recovery, and fluid loss control. Their results showed that the average tensile strength of saturated WC samples increased 26.33–51.33% from those of samples under ambient treatment (i.e., no heat treatment and no fluid saturation). EF results were less straightforward; they displayed average tensile strength increases of 3.94 and 6.79%, as well as average tensile strength decreases of 3.13 and 15.35%. Iferobia et al. (2022) suspected the adhesive nature of linear fracturing fluid to possibly cause compaction of shale grains leading to increased average tensile strength values when shale samples had a lower average percentage of increased mass. Conversely, when samples exhibited greater values of average percentage of increased mass, they hypothesized reduced linear fracturing fluid adhesiveness, weakened grain bonding, and the lowering of average tensile strength values. After fluid saturation, WC samples experienced an overall smaller increased mass percentage and greater tensile strength values compared to EF samples. The resulting mass percentage increase was higher and more variable for EF samples likely contributing to less uniform tensile strength conclusions. Though UICP promoting fluids were not used by Iferobia et al. (2022), they reveal that the shale rock matrix can be altered, positively and/or negatively, by foreign fluid exposure.

Shale, in general, is a heterogeneous material made up of diverse lithologies and mineral contents that result in highly variable rock matrices between and within shale types. Figure 18 (modified from Mews et al. (2019)) shows the variability in mineral content (percentage of carbonates, silicates, and clay) for shales used in this study: WC, EF, and Marcellus. Mews et al. (2019) reviewed the complex relationship between shale rock brittleness and lithology, and divided shale formations into four mineral content categories: silicate dominated, carbonate dominated, clay dominated, and strongly heterogeneous formations (not primarily dominant in silicates, carbonates, or clays). Shale is more brittle (and a practical candidate for hydraulic fracturing) when predominantly composed of silicates and/or carbonates and, conversely, more ductile when clay dominated. Notably, mineral content can be vastly different between and within shale types and is influential to

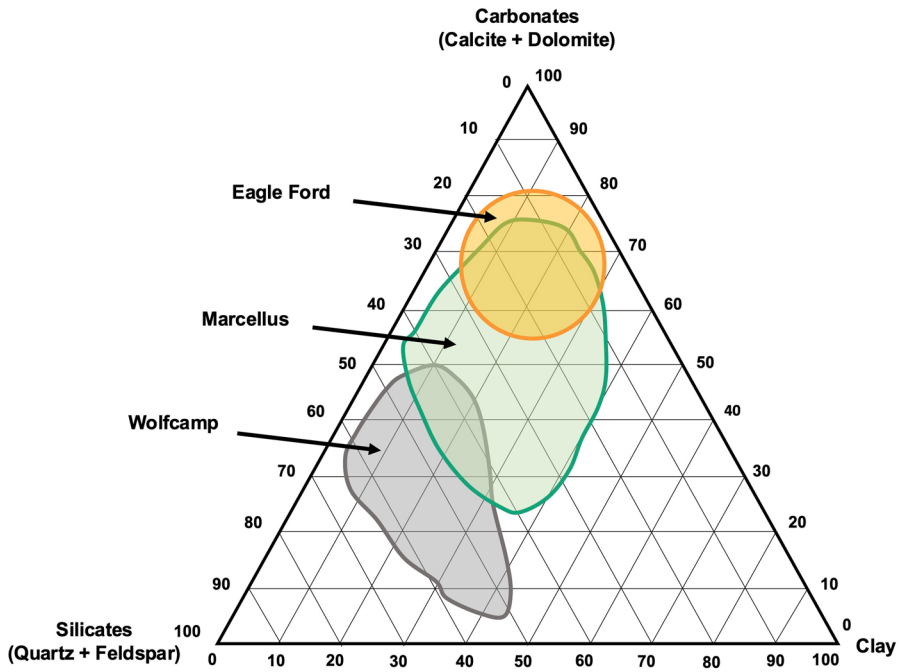

Fig. 18 Ternary diagram showing average mineral content for WC, EF, and Marcellus shales. Diagram modified from Mews et al (2019)

the ductility and/or brittleness of shale samples and likely a contributing factor to fracture behavior and tensile strength.

Anisotropy is a well-known characteristic of shale rock. The natural bedding planes found in shale introduce complexity to splitting tensile tests that is not inherent to isotropic rocks. BITS methods have been widely performed on different shale types to investigate tensile strength anisotropy and the effects of loading direction relative to the bedding plane of the sample (Gao et al. 2015; Jin et al. 2018; Li et al. 2017; Ma et al. 2018; Simpson et al. 2014; Wang et al. 2017). Wang et al. (2017) analyzed anisotropy in Longmaxi shale (cored parallel to the bedding plane) by changing the intersection angle between the bedding plane and loading direction in a series of BITS tests. Among other findings, their analysis indicated that (1) a 0° angle resulted in pure tensile failure in which fractures propagated along the bedding planes, (2) bedding planes experienced shear slippage when oriented and tested at a 30° angle, where a combination of shear and tensile mechanisms likely contributed to the failure, (3) at 90° the tensile strength was governed by the rock matrix when induced fractures crossed the shale and bedding planes, and (4) tensile strength was commonly higher when samples were oriented at 90° compared to 0°, suggesting weakness in the bedding plane laminations compared to the rock matrix. The intact EF and WC cores in this study were only tested with an intersection angle of 0° (Fig. 6a). Further tensile strength anisotropy was not evaluated or compared at other angles for samples cored parallel to the bedding plane. For the sealed cores, if the intersection angle between the loading direction and the sealed fracture was 0° (Fig. 6b, d), it is likely that the sealed fracture failed due to pure tensile stresses. However, for some of the less planar fractures (Fig. 12), a combination of shear and tensile mechanisms likely contributed to the failure. Other findings in the literature suggested differences in BITS between shale specimen cored perpendicular versus parallel to the bedding plane (Li et al. 2017; Wang et al. 2017). Strength was typically higher for specimens with perpendicular bedding planes where the applied BITS load crossed the bedding planes (Fig. 6c). Because only the two Marcellus cores in this study were cored perpendicular to the bedding planes the authors recognize that direct comparisons with the fractured and sealed EF cores are difficult to make. How bedding plane orientation influences the splitting tensile strength of fractured and sealed shale cores is complex and merits further experimentation.

Additionally, the single, heterogenous fracture along the length of the core was induced to reflect

fractures that might occur in subsurface formations during hydraulic fracturing. The fracture was not smooth and linear, rather rough and uneven, which introduced further heterogeneity to BITS testing where it was difficult to apply an evenly distributed load along the length of the biomineralized fracture. The heterogeneity of the lengthwise fracture also likely influenced biomineral formation inside the fracture. Willett et al. (2024) used NMR and CT, non-invasively, to show that biomineral formation inside a fracture is not homogeneous. Instead, mineral precipitation preferentially formed on and around proppant particles in flow-through, UICP-treated shale fractures, and primarily along the fracture edges in immersion UICP treatment. Additionally, in flow-through treatment, it was challenging to evenly distribute proppant and keep it stable within the fracture, leading to uneven mineral formation across the fracture aperture. The uneven mineral precipitation in both UICP treatment methods may contribute to a nonuniform mineral seal and a reduction in UICP-shale composite core strength, further increasing the heterogeneity of the BITS testing.

Moreover, cores sealed with the immersion method received one application of highly concentrated bacterial treatment ($OD_{600} > 1.8$), whereas flow-through cores received 20–30 sequential bacterial injections ($OD_{600} > 0.6$). Population assays of the two different bacterial concentrations have not been done to date, but the authors recognize the importance of performing this work. Highly concentrated bacterial treatments may not be appropriate for flow-through methods as the end of the core closest to the injection point notoriously experiences a decrease in permeability before other places in the fracture aperture. Rapid permeability reduction at the fracture influent is observed in other UICP treated fractured rock studies such as sealing fractured shale cores (Willett et al. 2024), fractured granite cores (Tobler et al. 2018), and fractured anhydrite with gouges (Sang et al. 2022). Increased bacterial concentrations may contribute to influent clogging phenomena causing a rapid decrease in fracture permeability without necessarily producing enough mineral deposits to hold the shale (or other rock or mineral type) together.

4 Conclusion

This work investigates tensile strength of fractured shale cores sealed with ureolysis-induced calcium carbonate precipitation (UICP). Tensile strengths were evaluated using a modified Brazilian indirect tensile strength (BITS) test on intact Eagle Ford (EF) and Wolfcamp (WC) cores at room temperature (RT) and 60 °C. The goal was to determine whether tensile strength was influenced by shale type and/or testing temperature conditions. Comparatively, UICP was delivered to fractured EF and Marcellus cores using either the flow-through or immersion method. The resulting composite cores were evaluated for tensile strength to understand the influence of UICP on fractured shale. Several conclusions can be made regarding this study:

- Intact WC shale exhibited more variability in tensile strength between replicates compared to intact EF shale. The authors suspect this is due to the existence of pre-existing fractures visible on the outside of the intact WC cores. This resulted in a wider standard deviation in the average tensile strength under both temperature conditions (RT or 60 °C). Visible pre-existing fractures were not evident on EF cores. However, statistical analysis did not indicate that shale type influenced tensile strength.
- The average tensile strength between temperature conditions appears to suggest that the shale in this study exhibits higher tensile strength at RT rather than 60 °C. Statistical analysis validated this finding between EF sample groups but challenged it between WC sample groups.
- All statistical models were verified to meet assumptions of constant variance and normality; however, the authors recognize that statistical differences between testing conditions are difficult to establish due to the small number of replicates in each shale type and temperature condition sample group.
- Shale cores can be sealed using a variety of UICP treatment delivery methods: flow-through and batch, immersion methods.
- The flow-through method successfully sealed all attempted core replicates with UICP and achieved three orders of magnitude permeability reduction inside the fracture.

- Two out of the three flow-through cores experienced biomineral cohesion within the fracture after BITS testing.
- Not all immersion method fracture treatments (specifically, M and CM treatments) were capable of sealing shale cores.
- Immersion method fracture treatments that included guar gum (GM and CGM treatments) sealed all core replicates at both RT and 60 °C. A total of 14 cores (four with the GM treatment and 10 with the CGM treatment) were sealed with the immersion method.
- Cores sealed at RT with the GM fracture treatment (no cells) experienced fracture treatment cohesion after BITS testing whereas those sealed with GM at 60 °C did not.
- Cores sealed with UICP and tested at 60 °C (under either flow-through or immersion method delivery) exhibited more mineral cohesion (~60%) after mechanical testing than cores sealed and tested at RT (20%).

Future work should further investigate guar gum as an additive to UICP treatment. This could involve performing flow-through sealing experiments where guar gum is added to UICP promoting fluids and the strength contribution of guar gum is examined. Future studies should include sealing cores from a wider variety of commonly fractured, hydrocarbon-rich shale formations to assess if UICP is compatible with other shale lithologies. Testing fractured and sealed cores for fracture toughness would be a suitable complement to the splitting tensile strength data. A complex investigation into bedding plane effects of fractured and sealed cores would be a suitable inclusion to understand the additional anisotropy introduced by the fracturing and sealing process. Finally, additional research into UICP's sealing capabilities under extreme subsurface conditions (i.e., overburden pressure and higher temperature) should be investigated before being applied to field application.

Acknowledgements The authors acknowledge the SubZero Science and Engineering Research facility at Montana State University for use of the MTS Criterion Model 43 testing apparatus. The authors would like to thank the Montana State University Machining Laboratory for collaboration and use of their facilities. This study was supported by funding from the US Department of Energy, Office of Basic Earth Sciences, DOE Award No.: DE-SC0021324. Additional funding for the LBNL author was provided by the U.S. Department of Energy under contract No. DE-AC0205CH11231 to the Lawrence Berkeley National Laboratory. Any opinions, findings, conclusions, or recommendations expressed herein are those of the authors and do not necessarily reflect the views of the Department of Energy (DOE).

Author contributions Conceptualization and Funding Acquisition: CMK, AJP, ABC, DC, JR. Methodology: KB, MRW, CMK, AJP, ABC. Experimentation and Data Collection: KB, MRW. Data Analysis: KB, CMK, AJP, KM, ABC. Writing—original draft preparation: KB. Writing—review and editing: MRW, CMK, AJP, KM, ABC, DC, JR. All authors approve of the content of the manuscript.

Funding This study was supported by funding from the US Department of Energy, Office of Basic Earth Sciences, DOE Award No.: DE-SC0021324. Additional funding for the LBNL author was provided by the U.S. Department of Energy under contract No. DE-AC0205CH11231 to the Lawrence Berkeley National Laboratory.

Availability of data and materials No datasets were generated or analysed during the current study.

Declarations

Ethics approval and consent to participate The authors declare that this paper does not involve ethical issues.

Consent for publication All the authors have approved the manuscript for submission and publication.

Competing interests The authors declare no competing interests.

References

Achal V, Mukerjee A, Sudhakara Reddy M (2013) Biogenic treatment improves the durability and remediates the

cracks of concrete structures. Constr Build Mater 48:1–5. https://doi.org/10.1016/j.conbuildmat.2013.06.061

ASTM (2008) D2936-20 standard test method for direct tensile strength of intact rock core specimens. In: West Conshohocken, PA, USA: ASTM International

ASTM (2016) D3967-08 standard test method for splitting tensile strength of intact rock core specimens. In: West Conshohocken, PA, USA: ASTM International

Barati R, Liang JT (2014) A review of fracturing fluid systems used for hydraulic fracturing of oil and gas wells. J Appl Polym Sci. https://doi.org/10.1002/app.40735

Bisai R, Chakraborty S (2019) Different failure modes of sandstone and shale under Brazilian tensile tests. J Adv Geotechn Eng 2(2):1–8. https://doi.org/10.5281/zenodo.3362989

Cui MJ, Zheng JJ, Zhang RJ, Lai HJ, Zhang J (2017) Influence of cementation level on the strength behaviour of bio-cemented sand. Acta Geotech 12(5):971–986. https://doi.org/10.1007/s11440-017-0574-9

Cladouhos T, Petty S, Swyer MW, Uddenberg ME, Grasso K, Nordin Y (2016) Results from Newberry Volcano EGS demonstration, 2010–2014. Geothermics 63(2016):44–61. https://doi.org/10.1016/j.geothermics.2015.08.009

Crandall D, Mackey P, Paronish T, Brown S, Moore J, Workman S, Warden L (2019) Computed Tomography Scanning and Geophysical Measurements of the Rhinestreet and Marcellus Shale from the Yawkey #98 Well. NETL-TRS-1–2019; NETL Technical Report Series; U.S. Department of Energy, National Energy Technology Laboratory: Morgantown, WV, 2019; p 44. https://doi.org/10.18141/1502092

Cunningham AR, Gerlach R, Philipps A, Lauchnor E, Rothman A, Hiebert R, Busch A, Lomans B, Spangler L (2015) Assessing potential for biomineralization sealing in fractured shale at the Mont Terri underground research facility, Switzerland. In: Gerdes KF (ed) Carbon dioxide capture for storage in deep geological formations: results from the CO_2 capture project, vol 4. CPL Press, pp 887–903

Cuthbert MO, McMillan LA, Handley-Sidhu S, Riley MS, Tobler DJ, Phoenix VR (2013) A field and modeling study of fractured rock permeability reduction using microbially induced calcite precipitation. Environ Sci Technol 47(23):13637–13643. https://doi.org/10.1021/es402601g

Deng J, Deng H, Zhang Y, Luo Y (2022) Experimental study on microbial-induced calcium carbonate precipitation repairing fractured rock under different temperatures. Sustainability 14(18):11770. https://doi.org/10.3390/su141811770

Dowling NE, Kral MV, Kampe SL (2019) Mechanical behavior of materials: engineering methods for deformation, fracture, and fatigue. Pearson Education, Incorporated

Espinoza DN, Santamarina JC (2017) CO2 breakthrough-caprock sealing efficiency and integrity for Carbon geological storage. Int J Greenhouse Gas Control 66:218–229. https://doi.org/10.1016/j.ijggc.2017.09.019

Gao Q, Tao JL, Hu JY, Yu X (2015) Laboratory study on the mechanical behaviors of an anisotropic shale rock. J Rock Mech Geotechn Eng 7(2):213–219. https://doi.org/10.1016/j.jrmge.2015.03.003

Ghasemi P, Montoya BM (2022) Field implementation of microbially induced calcium carbonate precipitation for surface erosion reduction of a coastal plain sandy slope. J Geotechn Geoenviron Eng 148(9):04022071. https://doi.org/10.1061/(asce)gt.1943-5606.0002836

Gomez MG, Anderson CM, Graddy CMR, DeJong JT, Nelson DC, Ginn TR (2017) Large-scale comparison of bioaugmentation and biostimulation approaches for biocementation of sands. J Geotechn Geoenviron Eng 143(5):04016124. https://doi.org/10.1061/(asce)gt.1943-5606.0001640

Halder BK, Roy D, Tandon V, Ramana CV, Tarquin AJ (2014) Use of mutated micro-organism to produce sustainable mortar. Aci Mater J 111(5):511–519. https://doi.org/10.14359/51686597

He JM, Afolagboye LO (2018) Influence of layer orientation and interlayer bonding force on the mechanical behavior of shale under Brazilian test conditions. Acta Mech Sin 34(2):349–358. https://doi.org/10.1007/s10409-017-0666-7

Hiebert R (2019) Phase 1 SBIR Final Report: Permeability control for enhanced oil and gas recovery in unconventional reservoirs using advanced mineral precipitation technologies

Hou B, Zeng YJ, Fan M, Li DD (2018) Brittleness evaluation of shale based on the Brazilian splitting test. Geofluids. https://doi.org/10.1155/2018/3602852

Iferobia CC, Ahmad M, Ali I (2022) Experimental investigation of shale tensile failure under thermally conditioned linear fracturing fluid (LFF) system and reservoir temperature controlled conditions. Polymers. https://doi.org/10.3390/polym14122417

Jin ZF, Li WX, Jin CR, Hambleton J, Cusatis G (2018) Anisotropic elastic, strength, and fracture properties of Marcellus shale. Int J Rock Mech Min Sci 109:124–137. https://doi.org/10.1016/j.ijrmms.2018.06.009

Kirkland CM, Akyel A, Hiebert R, McCloskey J, Kirksey J, Cunningham AB, Gerlach R, Spangler L, Phillips AJ (2021) Ureolysis-induced calcium carbonate precipitation (UICP) in the presence of CO2-affected brine: a field demonstration. Int J Greenhouse Gas Control 109:103391. https://doi.org/10.1016/j.ijggc.2021.103391

Kirkland CM, Thane A, Hiebert R, Hyatt R, Kirksey J, Cunningham AB, Gerlach R, Spangler L, Phillips AJ (2020) Addressing wellbore integrity and thief zone permeability using microbially-induced calcium carbonate precipitation (MICP): a field demonstration. J Pet Sci Eng 190:107060. https://doi.org/10.1016/j.petrol.2020.107060

Kong L, Ostadhassan M, Tamimi N, Samani S, Li C (2019) Refracturing: well selection, treatment design, and lessons learned—a review. Arab J Geosci 12(4):117. https://doi.org/10.1007/s12517-019-4281-8

Krajewska B (2009) Ureases I. Functional, catalytic and kinetic properties: a review. J Mol Catal B-Enzymatic 59(1–3):9–21. https://doi.org/10.1016/j.molcatb.2009.01.003

Li H, Lai B, Liu HH, Zhang J, Georgi D (2017) Experimental investigation on Brazilian tensile strength of organic-rich gas shale. SPE J 22(1):148–161. https://doi.org/10.2118/177644-pa

Lin H, Suleiman MT, Brown DG, Kavazanjian E (2016) Mechanical behavior of sands treated by microbially

induced carbonate precipitation. J Geotechn Geoenviron Eng 142(2):04015066. https://doi.org/10.1061/(asce)gt.1943-5606.0001383

Lu C, Li Z, Wang J, Zheng Y, Cheng L (2023) An approach of repairing concrete vertical cracks using microbially induced carbonate precipitation driven by ion diffusion. J Build Eng 73:106798. https://doi.org/10.1016/j.jobe.2023.106798

Ma TS, Peng N, Zhu Z, Zhang QB, Yang CH, Zhao J (2018) Brazilian tensile strength of anisotropic rocks: review and new insights. Energies 11(2):304. https://doi.org/10.3390/en11020304

Mellor M, Hawkes I (1971) Measurement of tensile strength by diametral compression of discs and annuli. Eng Geol 5(3):173–225. https://doi.org/10.1016/0013-7952(71)90001-9

Mews KS, Alhubail MM, Barati RG (2019) A review of brittleness index correlations for unconventional tight and ultra-tight reservoirs. Geosciences 9(7):319. https://doi.org/10.3390/geosciences9070319

Minto JM, MacLachlan E, El Mountassir G, Lunn RJ (2016) Rock fracture grouting with microbially induced carbonate precipitation. Water Resour Res 52(11):8827–8844. https://doi.org/10.1002/2016WR018884

Mobley HLT, Hausinger RP (1989) Microbial ureases: significance, regulation and molecular characterization. Microbiol Rev 53(1):85–108. https://doi.org/10.1128/mmbr.53.1.85-108.1989

Mokhtari M, Honarpour MM, Tutuncu AN, Boitnott GN (2014) Acoustical and geomechanical characterization of eagle ford shale - anisotropy, heterogeneity and measurement scale. Paper presented at the SPE Annual Technical Conference and Exhibition, Amsterdam, The Netherlands, October 2014. https://doi.org/10.2118/170707-MS

Montoya BM, DeJong JT (2015) Stress-strain behavior of sands cemented by microbially induced calcite precipitation. J Geotechn Geoenviron Eng 141(6):04015019. https://doi.org/10.1061/(asce)gt.1943-5606.0001302

Park SS, Choi SG, Nam IH (2014) Effect of plant-induced calcite precipitation on the strength of sand. J Mater Civ Eng 26(8):06014017. https://doi.org/10.1061/(asce)mt.1943-5533.0001029

Petty S, Nordin Y, Glassely W, Cladouhos T (2013) Improving geothermal project economics with multi-zone stimulation: results from the newberry volcano EGS demonstration. In: Proceedings, 38th workshop on geothermal reservoir engineering Stanford University, Stanford, CA

Phillips AJ, Cunningham AB, Gerlach R, Hiebert R, Hwang CC, Lomans BP, Westrich J, Mantilla C, Kirksey J, Esposito R, Spangler L (2016) Fracture sealing with microbially-induced calcium carbonate precipitation: a field study. Environ Sci Technol 50(7):4111–4117. https://doi.org/10.1021/acs.est.5b05559

Phillips AJ, Gerlach R, Lauchnor E, Mitchell AC, Cunningham AB, Spangler L (2013a) Engineered applications of ureolytic biomineralization: a review. Biofouling 29(6):715–733. https://doi.org/10.1080/08927014.2013.796550

Phillips AJ, Lauchnor E, Eldring J, Esposito R, Mitchell AC, Gerlach R, Cunningham AB, Spangler LH (2013b) Potential CO2 leakage reduction through biofilm-induced calcium carbonate precipitation. Environ Sci Technol 47(1):142–149. https://doi.org/10.1021/es301294q

Phillips AJ, Troyer E, Hiebert R, Kirkland C, Gerlach R, Cunningham AB, Spangler L, Kirksey J, Rowe W, Esposito R (2018) Enhancing wellbore cement integrity with microbially induced calcite precipitation (MICP): a field scale demonstration. J Petrol Sci Eng 171:1141–1148. https://doi.org/10.1016/j.petrol.2018.08.012

RCoreTeam (2022) R: a language and environment for statistical computing. R Foundation for Statistical Computing, Vienna, Austria. https://www.R-project.org/

Rutqvist J (2012) The geomechanics of CO2 storage in deep sedimentary formations. Geotech Geol Eng 30(3):525–551. https://doi.org/10.1007/s10706-011-9491-0

Sang G, Lunn RJ, Minto JM, Grainne El M (2022) Microbially induced calcite precipitation for sealing anhydrite fractures with gouges. Paper presented at the 56th U.S. Rock Mechanics/Geomechanics Symposium, Santa Fe, New Mexico, USA, June 2022. https://doi.org/10.56952/ARMA-2022-0277

Simpson NDJ, Stroisz A, Bauer A, Vervoort A, Holt RM (2014) Failure mechanics of anisotropic shale during Brazilian tests. Paper presented at the 48th U.S. Rock Mechanics/Geomechanics Symposium, Minneapolis, Minnesota, June 2014

Soeder DJ (2018) The successful development of gas and oil resources from shales in North America. J Petrol Sci Eng 163:399–420. https://doi.org/10.1016/j.petrol.2017.12.084

Stocks-Fischer S, Galinat JK, Bang SS (1999) Microbiological precipitation of CaCO3. Soil Biol Biochem 31(11):1563–1571. https://doi.org/10.1016/s0038-0717(99)00082-6

Tobler DJ, Minto JM, El Mountassir G, Lunn RJ, Phoenix VR (2018) Microscale analysis of fractured rock sealed with microbially induced CaCO3 precipitation: influence on hydraulic and mechanical performance. Water Resour Res 54(10):8295–8308. https://doi.org/10.1029/2018wr023032

Turner R, Castro GM, Minto J, El Mountassir G, Lunn RJ (2023) Treatment of fractured concrete via microbially induced carbonate precipitation: from micro-scale characteristics to macro-scale behaviour. Constr Build Mater 384:131467. https://doi.org/10.1016/j.conbuildmat.2023.131467

van Paassen LA, Ghose R, van der Linden TJM, van der Star WRL, van Loosdrecht MCM (2010) Quantifying biomediated ground improvement by ureolysis: large-scale biogrout experiment. J Geotechn Geoenviron Eng 136(12):1721–1728. https://doi.org/10.1061/(asce)gt.1943-5606.0000382

Vishal V, Rizwan M, Mahanta B, Pradhan SP, Singh TN (2022) Temperature effect on the mechanical behavior of shale: Implication for shale gas production. Geosyst Geoenviron 1(4):100078. https://doi.org/10.1016/j.geogeo.2022.100078

Wang Q, Chen X, Jha AN, Rogers H (2014) Natural gas from shale formation: the evolution, evidences and challenges of shale gas revolution in United States. Renew Sustain Energy Rev 30:1–28. https://doi.org/10.1016/j.rser.2013.08.065

Wang J, Xie LZ, Xie HP, Ren L, He B, Li CB, Yang ZP, Gao C (2016) Effect of layer orientation on acoustic emission characteristics of anisotropic shale in Brazilian tests. J Natl Gas Sci Eng 36:1120–1129. https://doi.org/10.1016/j.jngse.2016.03.046

Wang Y, Li CH, Hu YZ, Mao TQ (2017) Brazilian test for tensile failure of anisotropic shale under different strain rates at quasi-static loading. Energies 10(9):1324. https://doi.org/10.3390/en10091324

Whiffin VS, van Paassen LA, Harkes MP (2007) Microbial carbonate precipitation as a soil improvement technique. Geomicrobiol J 24(5):417–423. https://doi.org/10.1080/01490450701436505

Willett MR, Bedey K, Crandall D, Seymour JD, Rutqvist J, Cunningham AB, Phillips AJ, Kirkland CM (2024) Beyond the surface: non-invasive low-field NMR analysis of microbially-induced calcium carbonate precipitation in shale fractures. Rock Mech Rock Eng. https://doi.org/10.1007/s00603-024-04052-9

Xiao Y, Wang Y, Desai CS, Jiang X, Liu HL (2019) Strength and deformation responses of biocemented sands using a temperature-controlled method. Int J Geomech 19(11):04019120. https://doi.org/10.1061/(asce)gm.1943-5622.0001497

Yao X, Huafeng D, Jianlin L, Xingzhou C (2022) Shear performance and reinforcement mechanism of MICP-treated single fractured sandstone [Original Research]. Front Earth Sci. https://doi.org/10.3389/feart.2022.905940

Yasuhara H, Neupane D, Hayashi K, Okamura M (2012) Experiments and predictions of physical properties of sand cemented by enzymatically-induced carbonate precipitation. Soils Found 52(3):539–549. https://doi.org/10.1016/j.sandf.2012.05.011